Supplementary Information: Elucidating and Decoupling Diverse Fatigue Mechanisms Toward Static Self-Recovery in ZrO_2-Based Antiferroelectrics

Haoji Qian[1], Rongzong Shen[2], Jiacheng Xu[2], Miaomiao Zhang[1], Minglei Ma[1], Yian Ding[1], Xiaoxi Li[1], Gaobo Lin[2], Jiani Gu[2], Ran Cheng[3], Yan Liu[1], Chengji Jin[1,*], Jiajia Chen[1,*], Yue Hao[1], and Genquan Han[1]

[1]Hangzhou Institute of Technology and Faculty of Integrated Circuit, Xidian University, Xi'an 710071, China

[2]Center of Computational Materials, Zhejiang Lab, Hangzhou 311121, China

[3]College of Integrated Circuits, Zhejiang University, Hangzhou 310058, China

*E-mail: cjjin@xidian.edu.cn, chenjiajia@xidian.edu.cn

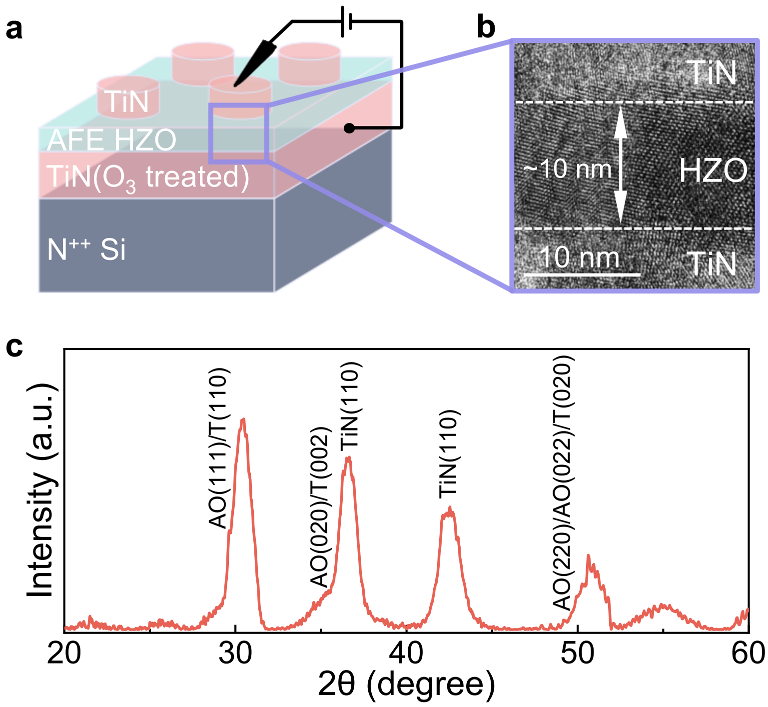

Supplementary Figure 1 Structural Characteristics. a, Schematic illustration of the AFE TiN/HZO/TiN capacitors. **b**, Cross-sectional TEM images of the HZO film. **c**, GIXRD spectra measured for a ZrO_2 capacitor.

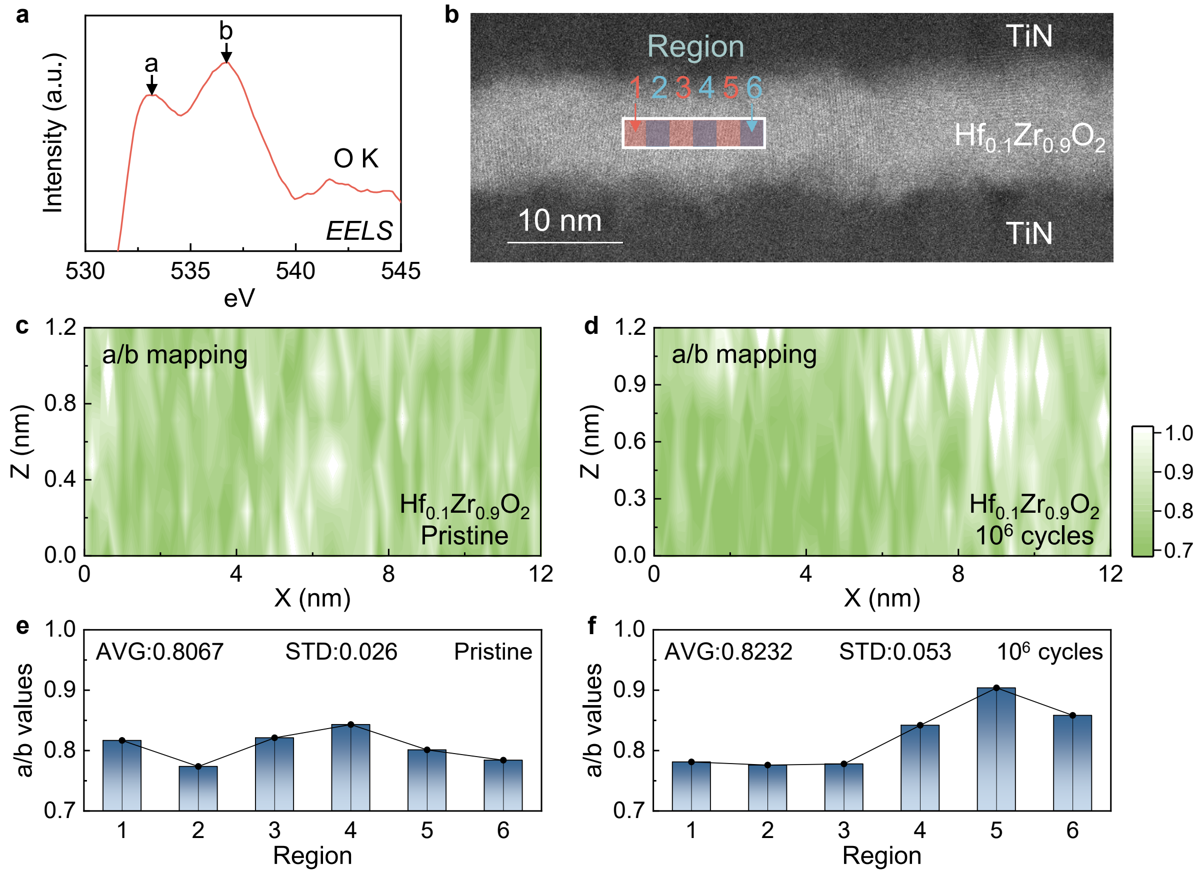

Supplementary Figure 2 Evolution of V_O distribution in $Hf_{0.1}Zr_{0.9}O_2$ capacitors. a, Typical O K EELS spectra averaged over the $Hf_{0.1}Zr_{0.9}O_2$ film. **b**, Device structure of $Hf_{0.1}Zr_{0.9}O_2$ capacitors and the schematic regions for EELS mapping. **c**,**d**, Maps of *a*/*b* ratio in O K EELS for pristine and 10^6 cycled $Hf_{0.1}Zr_{0.9}O_2$ samples, respectively. **e**,**f**, The average *a*/*b* ratio and standard deviation over region 1-6 of the pristine and 10^6 cycled $Hf_{0.1}Zr_{0.9}O_2$ samples, respectively.

The electron energy loss spectroscopy (EELS) analysis is performed to investigate the oxygen vacancies (V_O) distribution in $Hf_{0.1}Zr_{0.9}O_2$ capacitors before and after electrical cycling. The energy-loss near-edge structure (ELNES) of the oxygen (O) K-edge obtained from EELS spectrum imaging is analyzed. As reported in prior studies[1], the O K-edge typically exhibits a characteristic doublet with peaks labeled *a* (~534 eV) and *b* (~538 eV), which is shown in Supplementary Figure 2a. The relative intensity ratio of the peak *a* and *b* (*a*/*b*) is highly sensitive to the local chemical environment and coordination symmetry. A more uniform and stoichiometric O distribution tends to produce a well-defined doublet with balanced *a*/*b* values. In contrast, the presence of V_O and structural disorder such as those induced by cycling can lead to a suppressed peak *a*, resulting in a smaller *a*/*b* ratio.

As shown in Supplementary Figure 2c, the EELS mapping of pristine $Hf_{0.1}Zr_{0.9}O_2$ AFE film reveals a relatively uniform distribution of V_O, which correlates with the narrow full width at half maximum (*FWHM*) observed in the initial *I–V* characteristics. After 10^6 electrical cycles, the EELS mapping shows a clear localization of V_O, consistent with the broader *FWHM* measured after cycling (Supplementary Figure 3d). The detailed average (AVG) and standard deviation (STD) over Region 1-6 of the pristine and 10^6 cycled states are shown in Supplementary Figure 2e and Supplementary Figure 2f. This spectral evolution provides direct experimental evidence for the redistribution of V_O, and supports our explanation of the *FWHM* broadening observed in the electrical measurements.

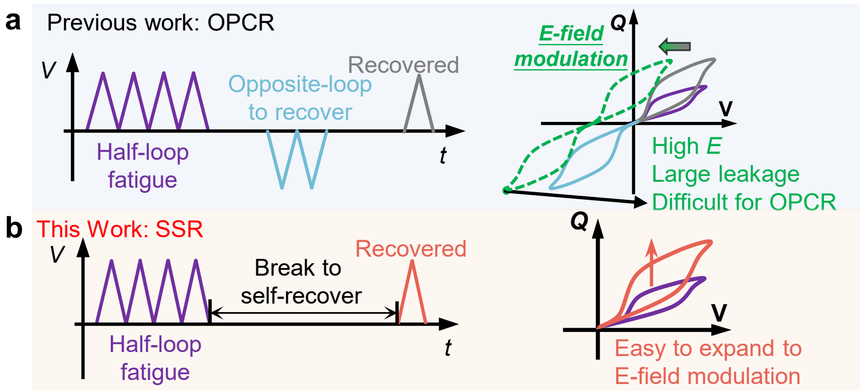

Supplementary Figure 3 Comparison between the OPCR and SSR recovery methods. a, Schematic illustration of previously proposed OPCR method in ref. 20. The half-loop fatigue is recovered by applying opposite-loop pulses, leading to large leakage for the requirement of a high electric field, and limiting its practical applicability. **b**, Schematic illustration of the SSR method proposed in this work. Allowing the device to self-recover after a break period following half-loop fatigue, simplifying the recovery process.

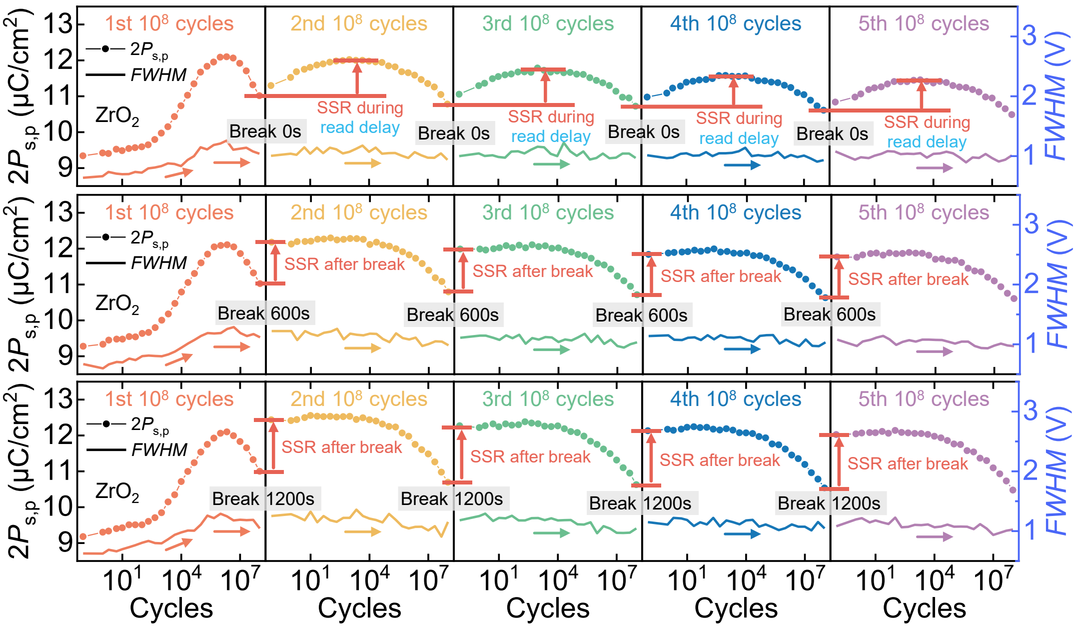

Supplementary Figure 4 The evolutions of $2P_{s,p}$ and the corresponding *FWHM* during continous four SSR processes in ZrO_2 capacitors, with the T_b set as 0/600/1200 s.

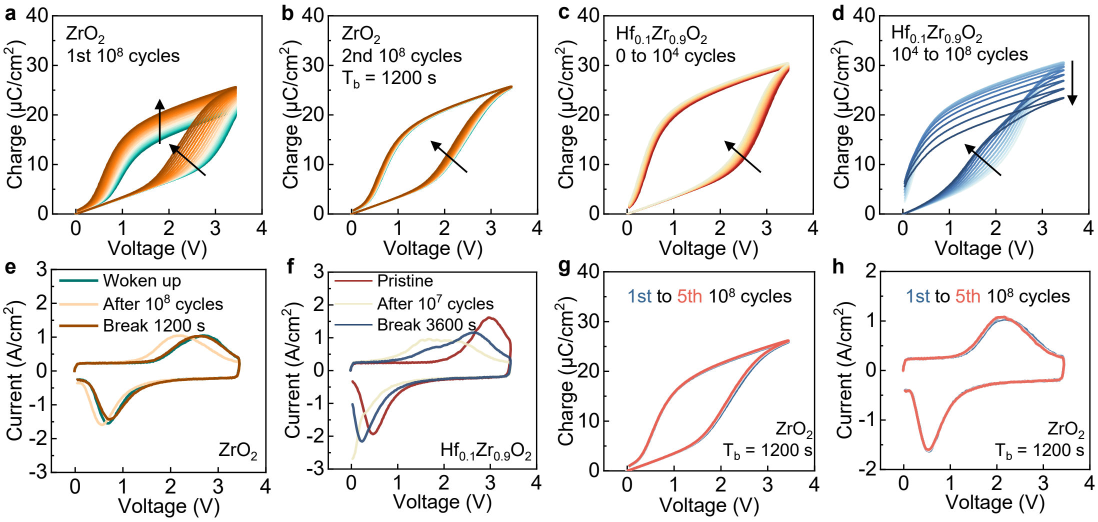

Supplementary Figure 5 Evolutions of the *Q*–*V* curves for ZrO_2 and $Hf_{0.1}Zr_{0.9}O_2$ capacitors. a, Evolution of the *Q*−*V* curves during the 1st 10^8 electrical cycles for ZrO_2 capacitors. **b**, Evolution of the *Q*−*V* curves during the 2nd 10^8 electrical cycles after SSR process with T_b = 1200 s for ZrO_2 capacitors. **c**, Evolution of the *Q*−*V* curves during the 0 to 10^4 electrical cycles for $Hf_{0.1}Zr_{0.9}O_2$ capacitors. **d**, Evolution of the *Q*−*V* curves during the 10^4 to 10^8 electrical cycles for $Hf_{0.1}Zr_{0.9}O_2$ capacitors. **e**,f, *I*−*V* curves of ZrO_2 and $Hf_{0.1}Zr_{0.9}O_2$ capacitors in the states before cycling, after cycling, and after SSR. **g,h,** *P*−*V* and *I*−*V* curves of 1st to 5th 10^8 electrical cycles for ZrO_2 capacitors.

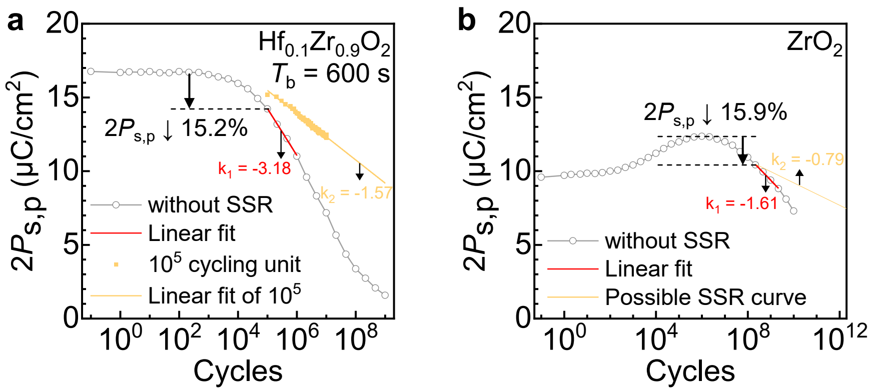

Supplementary Figure 6 Fatigue mitigation in $Hf_{0.1}Zr_{0.9}O_2$ and ZrO_2 AFE capacitors via SSR strategy. **a**, Endurance performances of $Hf_{0.1}Zr_{0.9}O_2$ samples, comparing the experimental measured data up to 10^9 electrical cycles (grey curve) and the linear fitting for the T_b = 600 s, cycling unit = 10^6 SSR combinations by extrapolating the results in Fig. 5d to 10^9 cycles. The fatigue rate is quantified by k_1 and k_2. **b**, Endurance performances of ZrO_2 samples, showing experimental measured data up to 10^{10} electrical cycles (grey curve), the linear fitted fatigue trend at 2×10^8 cycles without SSR (red curve) and the projected fatigue behavior under SSR application.

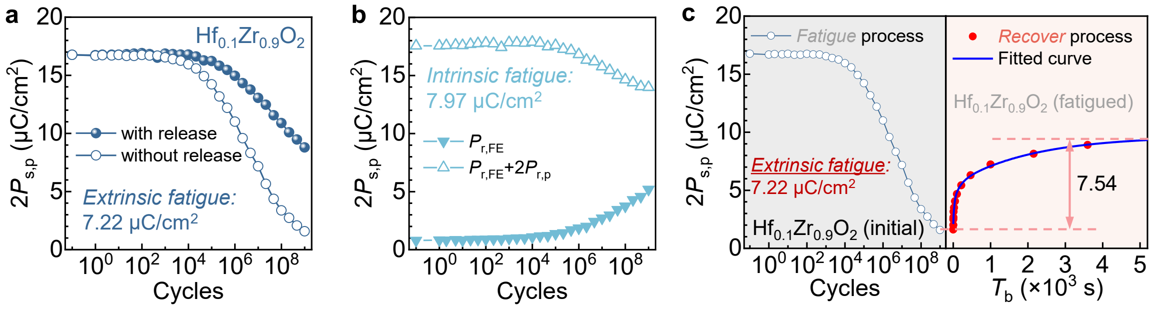

Supplementary Figure 7 SSR characteristics and fatigue mechanisms analysis for $Hf_{0.1}Zr_{0.9}O_2$ capacitors with 10^9 electrical cycles. a, Endurance characteristics of the $Hf_{0.1}Zr_{0.9}O_2$ capacitors, with and without charge release. **b**, Evolution of $P_{r,FE}$ and $P_{r,FE}+2P_{s,p}$ read by PUND and uni-PUND methods during 10^9 electrical cycling. **c**, Fatigue and recover processes of $Hf_{0.1}Zr_{0.9}O_2$ capacitors under 10^9 cycles, with T_b of 3600 s

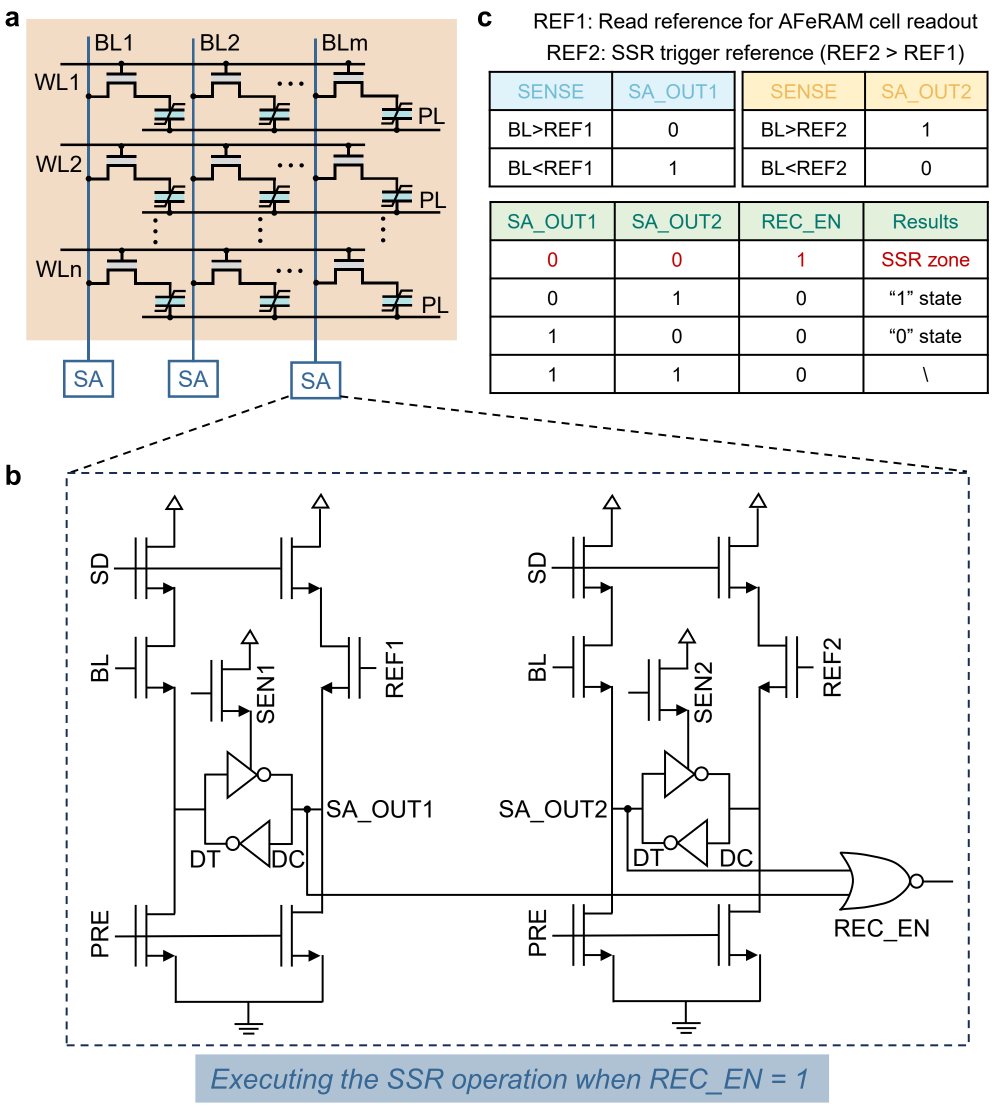

Supplementary Figure 8 Self-sensing circuit for SSR operation. a, Circuit architecture of ZrO_2-based AFeRAM array cooperated with **b**, sensing amplifiers to achieve self-sensing SSR scheme. **c**, SSR operation will be triggered when the output of REC_EN is "1".

As illustrated in Supplementary Figure 8, a self-sensing circuit for static self-recovery (SSR) operation has been designed. This circuit enables dynamic detection of the polarization degradation level by leveraging differential sensing through two reference cells. The circuit utilizes two sets of sense amplifier (SA) connected to reference cells. REF1 and REF2 represent the minimum signal of the "1" state and the sensed signal for executing the SSR operation, respectively. The design enables the delimitation of a degradation zone by comparing the outputs of the two SAs during a controlled read operation. Specifically, the reference cells are selected such that their readout voltages reflect different degradation thresholds. The output pattern (SA_OUT1 = 0, SA_OUT2 = 0) corresponds to a condition where the degraded target cell has crossed the predefined threshold, while the fresh cell remains readable. This pattern defines the SSR zone, indicating that the memory cell has entered a state requiring recovery. Once the SSR zone is detected, a recovery enable signal (REC_EN = 1) is asserted through a NOR gate, and the system can initiate appropriate SSR actions to recover the target cell. The detection logic is implemented using a simple digital comparator and control circuitry, allowing seamless integration into existing memory read paths. This design provides a practical and scalable solution for in-situ degradation monitoring, and aligns with the concept of self-tracking recovery proposed in ref. 2, while being tailored to our memory architecture.

References

1. Kang, D., Lee, S., Kim, Y. et al. Highly enhanced ferroelectricity in HfO_2-based ferroelectric thin film by light ion bombardment. *Science* **376**, 731–738 (2022).

2. Wu, C. et al. Robust Recovery Scheme for MFIS-FeFETs at Optimal Timing with Prolonged Endurance: Fast-Unipolar Pulsing (100 ns), Nearly Zero Memory Window Loss (0.02 %), and Self-Tracking Circuit Design. in *2023 International Electron Devices Meeting (IEDM)* 18.2.1-18.2.4 (IEEE, San Francisco, CA, USA, 2023).